Hydrogen diffusion in the protonic conductor $BaCe_{1-x}Gd_xO_{3-\frac{x}{2}}$ from density functional theory

Jessica Hermet,[1,2] Marc Torrent,[1] François Bottin,[1] Guilhem Dezanneau,[2] and Grégory Geneste[1,*]
[1]*CEA, DAM, DIF, F-91297 Arpajon, France*
[2]*Laboratoire Structures, Propriétés et Modélisation des Solides, UMR CNRS 8580, École Centrale Paris, Grande Voie des Vignes, 92295 Châtenay-Malabry Cedex, France*
(Received 1 January 2013; revised manuscript received 28 February 2013; published 22 March 2013)

The diffusion barriers of protonic defects in Gd-doped $BaCeO_3$, a compound candidate as electrolyte for protonic ceramic fuel cells, have been investigated by density functional theory calculations, starting from a previously computed energy landscape consisting of 16 kinds of stable sites (eight close to dopants and eight far from them). The simplified string method has been used to determine accurately the minimum energy paths between those sites that might imply either proton reorientations, intraoctahedral, or interoctahedral hopping mechanisms. At contrast with simple cubic perovskites such as barium stannate or barium zirconate, very different values for energy barriers (from 0.02 to 0.58 eV) are found in this highly distorted orthorhombic perovskite, and no specific process appears to be clearly rate limiting. Some interoctahedral hoppings (when possible) are found to be more favorable than the intraoctahedral ones, while reorientations exhibit a wide range of energy barriers.

DOI: 10.1103/PhysRevB.87.104303 PACS number(s): 66.30.Dn, 71.15.Mb

I. INTRODUCTION

Since the discovery of protonic conductivity in aliovalent-doped $SrCeO_3$,[1,2] protonic conduction in perovskite-type oxides ABO_3 has been the subject of numerous studies, experimental as well as computational.[3–7] The high protonic conductivity in perovskite oxides opens the way for a wide range of technological applications such as protonic ceramic fuel cells (PCFCs), hydrogen separators, etc. However, although the diffusion of protons has been extensively explored by *ab initio* calculations in cubic perovskites such as barium zirconate,[8,9] only very few works have studied this phenomenon in orthorhombic perovskites,[10] although excellent proton conductors, such as $SrCeO_3$ or $BaCeO_3$, present this symmetry at room temperature.

Proton conductors are usually obtained by replacing some cations of a host oxide compound by cations with lower valence. In perovskite oxides having a tetravalent element on the B site (Ti, Zr, Ce, Sn), this can be done by inserting on this site a trivalent element. Such substitution creates charge-compensating oxygen vacancies that make the compound reactive with respect to water dissociation if it is put in contact with humid atmosphere. Such hydration reaction is commonly written, using Kröger-Vink notations, as

$$H_2O + V_O^{\bullet\bullet} + O_O^X \rightarrow 2OH_O^{\bullet}. \quad (1)$$

It generates protonic defects $OH_O^{\bullet}$, localized approximately along [100]-type directions inside the interoctahedral space of the perovskite network, and that can move from an oxygen site to another by simple thermal activation. Three possible motions of the proton in the perovskite network have been distinguished: (i) the reorientation—the OH bond does not break and simply turns by $\approx 90^\circ$ around the B-O-B axis containing the oxygen atom; (ii) the intraoctahedral hopping—the proton leaves its oxygen site to move on another oxygen site of the same octahedron; (iii) the interoctahedral hopping—the proton leaves its oxygen site to move on another oxygen site that does not belong to the same octahedron.

In a previous work,[11] we have studied by density functional theory calculations the thermodynamics of hydration and oxidation of Gd-doped barium cerate $BaCe_{1-\delta}Gd_\delta O_{3-\frac{\delta}{2}}$ (BCGO). In particular, we have shown that hydration was an exothermic process and accurately determined the energy landscape of the proton near and far from the Gd dopant. We showed that this energy landscape can be well approximated by a surface with 16 kinds of local minima (eight in the close vicinity of the dopant and eight further). This complexity is the consequence of the highly distorted geometry of the host $BaCeO_3$ that adopts in its ground state the *Pnma* space group. Consequently, proton migration throughout such energy surface involves many different energy barriers that need to be explored in order to get insight into proton conduction at the macroscopic scale. Previous works have studied proton migration in $BaCeO_3$, but only in the cubic phase.[12–14] Therefore, in this work, we present an exhaustive study of the minimum energy paths associated to the possible motions for the proton in orthorhombic BCGO, and the values of their energy barriers.

II. COMPUTATIONAL DETAILS

A. Method

We have performed density functional theory (DFT) calculations using the plane-wave code ABINIT.[15,16] The generalized gradient approximation (GGA-PBE[17]) was employed to describe electronic exchange and correlation. The calculations were carried out in the framework of the projector augmented wave (PAW) approach.[18,19] The same supercell as that of Ref. 11 was used: it consists of 80 atoms and has an orthorhombic symmetry (*Pnma* space group). The first Brillouin zone of this supercell was sampled by a $2 \times 2 \times 2$ **k**-point grid, and the plane-wave cutoff was set to 20 Ha. The numerical accuracy on the total energies associated to this scheme is better than 1 mHa/atom. The cutoff radii of our PAW atomic data can be found in Ref. 11. All the calculations are spin-polarized.

In order to compute minimum energy paths, the first task was to identify the stable sites of the proton in BCGO, which was previously achieved in Ref. 11. This was performed by substituting in the 80-atom supercell one Ce by one Gd atom and introducing one hydrogen atom that was placed in its

different possible sites, close to the Gd dopant and far from it. In each configuration, the atomic positions were optimized until all the cartesian components of atomic forces were below 1×10^{-4} Ha/Bohr ($\approx$0.005 eV/Å).

The possible energy barriers between pairs of stable protonic sites have then been computed using the so-called simplified string method.[20,21] The simplified string method is an iterative algorithm allowing to find the minimum energy path (MEP) between two stable configurations. It consists in discretizing the path into equidistant configurations, that we call "images." At each iteration, a two-step procedure is applied: first, each image is moved along the direction given by the atomic forces (evolution step), then the images are redistributed along the path in order to be kept equidistant (reparametrization step). To determine the number of iterations of string method, we used an optimization criterion related to the energy of the images: the optimization of the MEP is stopped when the total energy (averaged over all the images) difference between an iteration and the previous one is lower than 1×10^{-5} Ha. In such an algorithm, the result should be carefully converged with respect to the number of images along the path, which forced us to use up to 19 images in the case of some intraoctahedral hopping processes. Once the MEP has been correctly converged, the maximum energy along the path provides us the transition state, and thus the energy barrier of the corresponding process (hopping or reorientation). Finally, we point out that all the atoms of the supercell were allowed to move during the computation of the MEP, thus providing energy barriers in a "fully relaxed" system.

For the sake of numerical efficiency, we have used the three traditional levels of parallelization present in the ABINIT code (**k** points, bands, plane waves) together with a fourth level on the images of the system used to discretize the MEP. This fourth level has a quasilinear scalability and, since the number of images used to discretize the path can be as large as 19, thousands of cpu cores can be used to compute and relax the MEP with high efficiency. Typical jobs were done on 3000 cpu cores using these four parallelization levels, allowing us to take maximal benefit of the potentialities of parallel supercomputers.

B. Approximations to the computation of energy barriers

Additional remarks have to be mentionned about the limits of our approach and the approximations made to compute the energy barriers. First of all, the string method, like the nudged elastic band method, allows to compute the MEP between two stable configurations and thus to obtain "fully relaxed" (static) barriers, as opposed to "dynamical" barriers that would be obtained, for instance, by counting the occurrences of each event within a molecular dynamics run and fitting the rates by an Arrhenius law. Static barriers neglect some collective effects and the so-called recrossing processes. In theory, they make sense only if the whole structure is able to relax instantaneously when the proton moves from a stable position to another. However, the time scale associated to the hydrogen motion is much smaller than the ones of the deformation of the surrounding structure, which involves much softer phonon modes. The motion of protons in an unrelaxed environment would naturally lead to higher barriers than those calculated from fully-relaxed DFT calculations. Nevertheless, as shown by Li and Wahnström[22] in metallic palladium, the jump of the proton has to be considered in a reverse way. Due to the vibrations of surrounding atoms and to the high vibration frequency of hydrogen, protons currently jump at a moment where the surrounding atoms are in a geometrical configuration close to the calculated relaxed one. Further work is necessary to verify that the proton jump, for instance, during *ab initio* molecular dynamics simulations, occurs for a geometry of surrounding atoms close to that calculated in the fully relaxed DFT static scheme.

Second, the present barriers do not include quantum zero-point energies. They are valid in the limit where nuclei can be considered as classical particles. If this approximation is correct for heavy atoms in the temperature range interesting PCFCs, this is not so obvious for the proton.[9] Indeed, proton tunneling might occur and thus significantly lower the barrier height, especially in the hopping case.[23] This approximation leads to overestimated barriers. Using typical values for the frequency of the stretching mode of the OH bond, it is possible to estimate this overestimation to $\approx$0.15 eV in the transfer case. The reorientation is less affected since OH is not broken during this mechanism.[23]

Last, the use of the generalized gradient approximation tends to underestimate the activation energy for proton transfer in hydrogen-bonded systems.[8] This underestimation is due to an overstabilization of structures in which a hydrogen is equally shared between two electronegative atoms.[24] This underestimation has been estimated in Ref. 24 to 0.10–0.15 eV by comparison between a standard GGA barrier and a B3LYP result.

Consequently, the barriers presented in this work purely reflect the GGA potential energy surface of the proton in its host compound. They are static barriers, free from collective, dynamical, and quantum effects. Quantum zero-point motions might lower the transfer barriers by $\approx$0.15 eV, the reorientation being almost not affected. On the other hand, a more accurate exchange-correlation energy functional would probably enhance the transfer barriers by $\approx$0.10–0.15 eV. We conclude that the barriers we compute using the previous approximations remain significant, keeping in mind that the error bar on the transfer barriers is higher than that on the reorientations.

III. REVIEW OF PRELIMINARY RESULTS: STRUCTURE OF $BaCeO_3$ AND PROTONIC SITES

A. $BaCeO_3$ and BCGO structures

As many perovskites,[25] $BaCeO_3$ has an orthorhombic structure ($Pnma$ space group[26]) at room temperature (RT). At high temperature, it undergoes three structural phase transitions, the first one at $\approx$550 K towards an $Imma$ structure and the second one at $\approx$670 K towards a rhombohedral $R\bar{3}c$ structure. At very high temperature ($\approx$1170 K), it evolves towards the parent $Pm\bar{3}m$ cubic structure, that of the ideal perovskite. The presence of dopants randomly distributed throughout the matrix may change transition temperatures. However, Melekh *et al.*[27] found that the first transition in 10%-Gd-doped $BaCeO_3$ occurs around 480–540 K, close to the one they found for pure $BaCeO_3$ of 533 K. At RT, Gd-doped $BaCeO_3$ is therefore orthorhombic.

Our calculations provide optimized configurations and MEP. These computations are thus relevant when performed in combination with the ground-state structure of $BaCeO_3$, i.e., the orthorhombic *Pnma* structure, which was used as starting point in all the calculations, and globally preserved along the optimizations procedures. The computed energy barriers can therefore be used to understand proton diffusion in BCGO below ≈550 K. However, from a more general point of view, the present results provide a useful microscopic insight into proton diffusion in a low-symmetry perovskite compound, typical of those used as electrolytes in proton ceramic fuel cells (the *Pnma* structure is common to many perovskites such as cerates, zirconates, titanates, or stannates).

The structural parameters obtained for $BaCeO_3$ and BCGO within the present scheme can be found in Ref. 11. They are in excellent agreement with experiments, despite a slight overestimation of the lattice constants related to the use of the GGA.

B. Protonic sites in perovskites: general considerations

As previously explained, proton conduction in an ABO_3 perovskite compound—where B is a tetravalent element—might be obtained by substituting B atoms by trivalent elements such as Gd (this creates oxygen vacancies by charge compensation) and by subsequently exposing this compound to humid atmosphere. The protons as charge carriers then appear through the dissociation of water molecules into the oxygen vacancies, according to the well-known hydration reaction [see Eq. (1)].

The precise location of the stable protonic sites in the perovskite network seems to strongly depend on the lattice parameter and distortion of the host compound. It is commonly admitted that protons are bonded to an oxygen atom and remain in the form of hydroxyl groups located on oxygen sites. But the orientation of the O-H bond is not that clear. On the one hand, it was proposed that it could be oriented along the BO_6 octahedra edge because of its dipolar moment,[6,28] leading to eight possible sites per oxygen atom. On the other hand, previous experimental[29] and *ab initio*[30–32] studies have found only four sites per oxygen atom oriented along the pseudocubic directions.

In fact, the stable protonic sites seem to be, indeed, (i) along or close to the octahedra edge for perovskites with relatively small lattice constant a_0, such as $SrTiO_3$[3,33] or $LaMnO_3$[3] ($a_0 = 3.91$ Å), leading to the existence of eight protonic sites per oxygen atom, (ii) along the pseudocubic directions for perovskites with large lattice constant, such as $SrZrO_3$[31] or $BaCeO_3$[11,30,32] (pseudocubic lattice constant $a_0 = 4.14$ and 4.41 Å, respectively), leading to the existence of four protonic sites per oxygen atom. This trend can easily be explained as the lattice constant decreases, the nearest oxygen gets closer and closer to the proton, attracting it sufficiently (through hydrogen bond) to bend the O-H bond towards the octahedron edge.

C. Protonic sites in Gd-doped $BaCeO_3$

In our previous calculations on BCGO,[11] which has a large pseudocubic lattice constant of 4.41 Å, we found indeed four stable protonic sites per oxygen atom. Considering that the *Pnma* structure contains two inequivalent oxygen atoms O1 and O2, this leads to the existence of eight inequivalent stable positions for the proton, if we ignore the symmetry-breaking caused by the presence of dopants. These positions have been labeled 1a, 1b, 1c, and 1d for those attached to O1 (apical oxygen), and 2a, 2b, 2c, and 2d for those attached to O2 (equatorial oxygen), see Fig. 1.

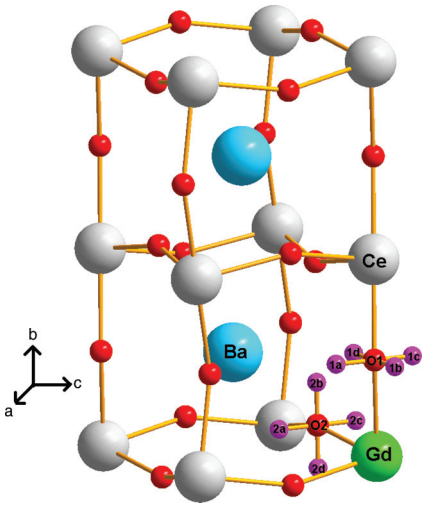

FIG. 1. (Color online) The eight stable positions for the proton around the Gd dopant, as computed in Ref. 11 and starting point of the present study.

However, when one Ce atom is replaced by a Gd dopant, both the translational symmetry and the symmetry between the four equatorial oxygens O2 of the first coordination shell of this specific B site are broken. More precisely, the presence of Gd splits the four O2 into two pairs of symmetry equivalent oxygen atoms (O2 and O2'). The four inequivalent protonic sites related to O2 (2a, 2b, 2c, and 2d) are thus split into eight inequivalent sites, called 2a, 2b, 2c, 2d, 2a', 2b', 2c', and 2d'. The first coordination shell of Gd exhibits therefore 12 kinds of inequivalent protonic sites. Beyond this shell, the symmetry breaking is even more complex.

Nevertheless, we have shown in Ref. 11 that this complex protonic energy landscape can be very well approximated by a surface containing 16 kinds of inequivalent local minima: eight corresponding to the eight sites shown in Fig. 1 close to a Gd dopant, and eight associated to the same sites "far" from the dopant, i.e., beyond its first oxygen coordination shell. Table I gives the relative energy associated to each site (taken

TABLE I. Energy (in eV) of the possible proton binding sites in BCGO relative to the most stable one (1an). The energies of the positions far from Gd are subject to an uncertainty of ≈0.02 eV according to their precise location (see text).

Gd-OH-Ce		Ce-OH-Ce	
1an	0.00	1af	0.09
1bn	0.01	1bf	0.08
1cn	0.11	1cf	0.25
1dn	0.00	1df	0.14
2an (2a'n)	0.17 (0.16)	2af	0.25
2bn (2b'n)	0.05 (0.05)	2bf	0.12
2cn (2c'n)	0.15 (0.13)	2cf	0.29
2dn (2d'n)	0.08 (0.09)	2df	0.23

TABLE II. Values of the angle described in Fig. 2, for a proton near a dopant and far from a dopant.

Position	θ near Gd	θ far from Gd
1a	−0.1°	0.2°
1b	−0.1°	0.2°
1c	5.3°	0.5°
1d	3.5°	0.5°
2a	−0.5°	0.6°
2b	1.6°	1.2°
2c	5.0°	2.1°
2d	8.2°	4.9°

from Ref. 11): in the first coordination shell of Gd, only eight sites among the 12 can be considered as nonequivalent. Beyond this first shell also, only the same eight kinds of sites can be considered as nonequivalent with a very good accuracy (≈0.02 eV). In other words, the symmetry breaking caused by the presence of dopants can be considered as having no significant influence on the energy landscape of the protonic defects. In order to distinguish the sites of these two families, we introduce another letter, "n" (for a site *near* the dopant) or "f" (for a site *far* from the dopant).

To summarize, the 16 kinds of stable positions are labeled by (1) a number (1 or 2) corresponding to the oxygen type (apical and equatorial, respectively), (2) a letter ("a," "b," "c," or "d") corresponding to the O-H direction (shown in Fig. 1), and (3) another letter, "n" for a site *near* the dopant, or "f" for a site *far* from the dopant.

In the presence of a dopant, the OH bond might slightly deviate from the pseudocubic direction: usually the proton is expected to bend towards the dopant due to the opposite formal charge of the corresponding defects (+1 for the protonic defect $OH_O^{\bullet}$ versus −1 for the dopant defect Gd'_{Ce}). But it also depends on the dopant size.[8,31]

In the present case, the proton has indeed a tendency to bend slightly towards the dopant, but with a deviation from the pseudocubic direction lower than 10° (see Table II). It is possible to divide the eight stable sites into two categories: either the proton is able to hop from one octahedron to another (a/b type) or not (c/d type). The c/d-type site shows a noticeable bending (around 5°), while the a/b-type are almost perfectly aligned along the pseudocubic direction. This absence of bending may be due to the stabilization of a/b-type sites by an hydrogen bond with the facing oxygen, which is in those cases rather close. This hydrogen bond would be dominant over the proton-dopant interaction, especially since the dopant is much further than for a c/d-type site (see Fig. 2).

Note that in perovskites with smaller lattice constant, the bending is usually stronger, but also highly dopant dependent. Bjorketun *et al.*[8] have studied this dependence in $BaZrO_3$ and got a bending angle from 6.9° for gadolinium up to 20.4° for gallium.

IV. ENERGY BARRIERS

We have seen that the energy landscape of stable protonic sites in Gd-doped $BaCeO_3$ is really complex, due to the distortions of the *Pnma* structure and the presence of dopants. As a result, there are many different values for the energy barriers, associated to several diffusion mechanisms, even by considering the simplified energy landscape (with 16 minima) presented previously.

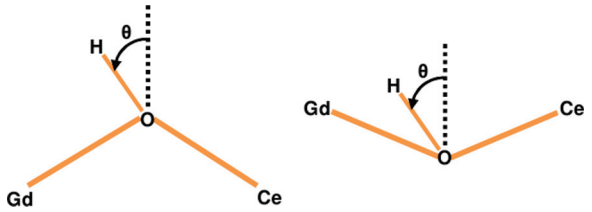

FIG. 2. (Color online) Angles between the pseudocubic direction and the actual O-H bond for the two subcategories of protonic sites (left: a/b-type; right: c/d-type).

A. The three different mechanisms: reorientation, intraoctahedral, and interoctahedral hopping

In an ideal cubic perovskite, there are two kinds of processes for the proton motion: reorientation and transfer (or hopping),[34] to which only two different energy barriers can be associated, provided the proton is assumed to be far from any dopant. In $BaZrO_3$,[35] the reorientation (respectively, transfer) barrier is 0.14 eV (respectively, 0.25 eV), while in cubic $BaTiO_3$,[35] it is 0.19 eV (respectively, 0.25 eV). In such simple systems, each proton in a stable site has four different possibilities to move: two reorientations and two intraoctahedral hoppings, the interoctahedral hopping being considered as unlikely (because the oxygen facing the OH group is too far).

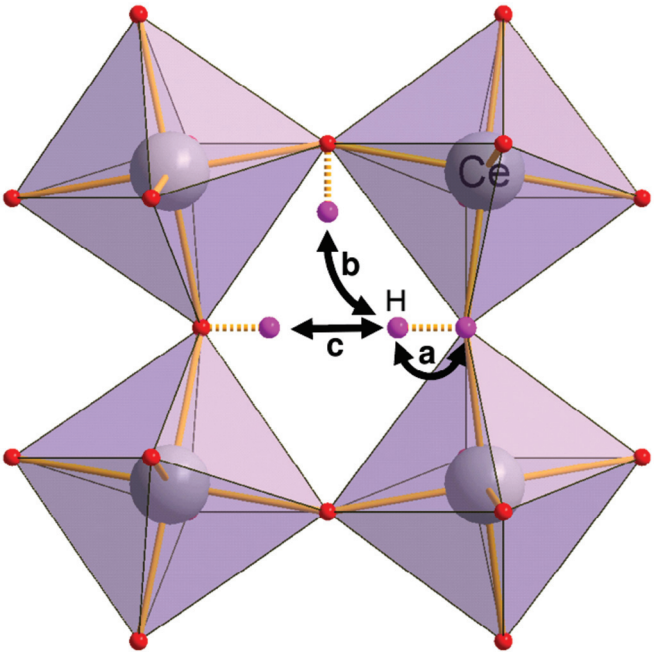

FIG. 3. (Color online) Possible motions of the proton in the perovskite *Pnma* structure: (a) reorientation, (b) intraoctahedral hopping, and (c) interoctahedral hopping.

TABLE III. Pseudocubic lattice constant a_0 from DFT calculations (GGA), tolerance factor t calculated from Shannon ionic radii, crystal space group of different perovskite oxides, and whether flip or interoctahedral hopping can occur or not according to cited works. For $BaTiO_3$, the high-temperature cubic structure is considered, which is the one simulated in Ref. 35. The cubic structure is also considered for $SrTiO_3$, rather than the low-temperature tetragonal structure. In those two cases, the ground-state space group is given between parentheses.

Perovskite	a_0 (Å)	t	Structure	Flip	Inter
$SrCeO_3$[39]	4.29	0.89	$Pnma$	no	yes
$CaZrO_3$[31,35,40,41]	4.04	0.92	$Pnma$	no	yes
$BaCeO_3$[39]	4.41	0.94	$Pnma$	no	yes
$SrZrO_3$[31,41,42]	4.14	0.95	$Pnma$	no	yes
$CaTiO_3$[14,35,37]	3.85	0.97	$Pnma$	yes	yes
$BaZrO_3$[34,35,41]	4.25	1.01	$Pm\bar{3}m$	no	no
$SrTiO_3$[14,37]	3.91	1.01	$Pm\bar{3}m$ ($I4/mcm$)	yes	no
$BaSnO_3$[43]	4.16	1.03	$Pm\bar{3}m$	no	no
$BaTiO_3$[35]	4.06	1.07	$Pm\bar{3}m$ ($R3m$)	no	no

However, the existence of tilts of oxygen octahedra, very common in perovskite oxides[25] having low tolerance factor $t = \frac{r_A + r_O}{\sqrt{2}(r_B + r_O)}$, makes the interoctahedral hopping more likely in these strongly distorted structures (see Fig. 3), because some interoctahedral oxygen-oxygen distances might be considerably lowered by the antiferrodistortive motions of the oxygen atoms. The proton may thus jump directly from one octahedron to another (one interoctahedral hopping instead of two intraoctahedral hoppings), which might result in an increase of the macroscopic diffusion coefficients. Table III emphasizes the link between the tolerance factor t, the perovskite structure, and the possibility of interoctahedral transfer according to the works mentionned.

As explained in Sec. III B, in perovskites with small lattice constant ($\leqslant$4.0 Å), the proton in its stable site tends to bend towards one oxygen atom of one neighboring octahedron instead of being equidistant from both neighboring oxygens. In such systems, there are therefore twice more stable sites than in perovskites with larger lattice constant, so that an additional rotational mechanism might exist, corresponding to the slight reorientation of OH, bending from the edge of one neighboring octahedron to the other. This mechanism was previously called "flip,"[36] "bending,"[12] or "interoctahedron hopping"[33] (but "interoctahedron reorientation" should be less confusing, since the bond between O and H is not broken during this process). However, the energy barrier of the flip is usually rather low ($\lesssim$0.1 eV[33]), and thus most of the time neglected. It can also be seen as part of the intraoctahedral transfer mechanism; before jumping from one oxygen to another, there is a little reorientation of the proton in order to get an alignment O-H. . .O. The intraoctahedral transfer would thus be a two-step mechanism with bending then stretching.

Table III illustrates the possible correlation between the lattice parameter and the possibility to flip for several proton conductor perovskites. Note that some studies found a possible interoctahedral transfer in small cubic perovskite such as $SrTiO_3$[5,14,37] or even in cubic perovskites with large lattice constant such as $BaZrO_3$,[38] in contradiction with other works.[14,35]

TABLE IV. Energy barriers (eV) for proton reorientation, intraoctahedral hopping ("intra") and interoctahedral hopping ("inter").

	Reorientation				Intra				Inter	
From	To	ΔE	To	ΔE	To	ΔE	To	ΔE	To	ΔE
1an	1bn	0.50	1dn	0.10	2dn	0.37	2df	0.58	1bf	0.24
1bn	1cn	0.30	1an	0.49	2dn	0.32	2df	0.48	1af	0.24
1cn	1dn	0.05	1bn	0.20	2bn	0.29	2bf	0.43		
1dn	1an	0.09	1cn	0.16	2bn	0.36	2bf	0.52		
2an	2bn	0.31	2dn	0.15	2cn	0.22	2cf	0.40	2af	0.25
2bn	2cn	0.28	2an	0.43	1cn	0.35	1cf	0.51	2bf	0.21
					1dn	0.31	1df	0.47		
2cn	2dn	0.03	2bn	0.18	2an	0.23	2af	0.45		
2dn	2an	0.23	2cn	0.09	1an	0.29	1af	0.44		
					1bn	0.24	1bf	0.39		
1af	1bf	0.54	1df	0.14	2df	0.50	2dn	0.44	1bf	0.19
									1bn	0.16
1bf	1cf	0.33	1af	0.54	2df	0.45	2dn	0.40	1af	0.20
									1an	0.16
1cf	1df	0.06	1bf	0.18	2bf	0.36	2bn	0.32		
1df	1af	0.08	1cf	0.15	2bf	0.42	2bn	0.39		
2af	2bf	0.36	2df	0.17	2cf	0.39	2cn	0.36	2af	0.21
									2an	0.17
2bf	2cf	0.33	2af	0.49	1cf	0.47	1cn	0.42	2bf	0.16
					1df	0.44	1dn	0.39	2bn	0.13
2cf	2df	0.02	2bf	0.17	2af	0.36	2an	0.28		
2df	2af	0.20	2cf	0.08	1af	0.37	1an	0.34		
					1bf	0.31	1bn	0.28		

B. Energy barriers and MEP

Using the string method, the MEP joining the various stable sites have been computed, giving access to the transition states and thus the energy barrier for the corresponding proton motion. These energy barriers are provided in Table IV. Note that the barriers far from dopants (i.e., from "f" to "f") have been also computed in an undoped 80-atom supercell in a $+1$ charge state (no Gd and one H inside), compensated by a uniform charged background. The energy barrier values obtained are identical to the ones obtained in the doped supercell within 0.01 eV and are presented in Appendix.

Starting from a given initial position, the possible motions for the proton are two reorientations, two intraoctahedral hoppings, and, possibly, one interoctahedral hopping if the configuration is favorable (which is the case for a and b-type positions where the oxygen atom facing the proton is close enough). Looking at Table IV, we can notice that barriers between two "near" sites or two "far" sites, corresponding to reorientation barriers, are very similar (difference within 0.05 eV). This is expected as the energy surface of protons bonded to an oxygen first neighbor of a dopant is almost simply shifted by 0.1 eV compared to that of protons far from the dopant, leading to similar energy landscape. However, the case of hopping is more complicated since the Coulomb interaction between H and Gd prevents hydrogen from easily escaping from the dopant neighborhood. Thus hopping barriers between a "near" site and a "far" site have usually a higher value that the ones corresponding to the backward motion.

Figure 4 illustrates the energy profile for each of the three possible kinds of mechanisms (note this is not an exhaustive list of all possible profiles): Fig. 4(a) shows the energy profile, as well as the evolution of the O-H distance and the angle ϕ from the initial O-H direction in the case of a complete turn around an oxygen O1 near the dopant. Using the notations of Table IV, it corresponds to the four reorientation mechanisms: 1an $\Rightarrow$ 1bn $\Rightarrow$ 1cn $\Rightarrow$ 1dn $\Rightarrow$ 1an. These four reorientation barriers have not the same profile at all: not only the barrier height can differ by a factor 5, but also the angle between two stable sites varies from 60° to 120° instead of being set to 90° (case of an ideal cubic perovskite). Figures 4(b) and 4(c) give similar information but for intraoctahedral and interoctahedral hoppings, respectively. Both mechanisms seem to occur in two steps: first a reorientation, slight for interoctahedral hopping ($\approx$5°) and larger for intraoctahedral hopping ($\approx$45°) in order to get O-H-O aligned, then the jump between both oxygen atoms. This reorientation can be related to what we mentioned as "flip" in the previous section.

V. DISCUSSION

A. Comparison between Gd-doped $BaCeO_3$ and In-doped $CaZrO_3$

The present results on Gd-doped $BaCeO_3$ can be compared with previous values computed in In-doped $CaZrO_3$,[10,40,44] as both materials exhibit the same kind of structural distortion: $BaCeO_3$ and $CaZrO_3$ have the same perovskite structure with very close Goldschmidt's tolerance factors (0.94 and 0.92, respectively) and thus have the same orthorhombic structure with P*nma* space group. However, according to its bigger tolerance factor, $BaCeO_3$ should be slightly less distorted from the cubic structure and thus interoctahedral transfer may be harder than in $CaZrO_3$. Table V confirms that $BaCeO_3$ is a bit closer to an ideal cubic structure than $CaZrO_3$.

TABLE V. Structural parameters (lattice parameters, cation-oxygen distances, and angles) for $BaCeO_3$, $CaZrO_3$, and a fictitious cubic perovskite.

	$BaCeO_3$	$CaZrO_3$[10]	cubic
a_c (Å)	4.44	4.06	...
a/a_c	1.41	1.39	1.41
b/a_c	1.42	1.44	1.41
c/a_c	2.00	2.00	2.00
$\overline{\text{A-O}}/a_c$ ($\pm\sigma$)	0.71 ($\pm$0.21)	0.72 ($\pm$0.22)	0.71
$\overline{\text{B-O}}/a_c$ ($\pm\sigma$)	0.51 ($\pm$0.00)	0.52 ($\pm$0.00)	0.50
A-O-A (deg)	153.85	144.74	180.00
B-O-B (deg)	156.45	145.49	180.00

The same tendency is indeed observed with a very large range of possible values for energy barriers from a few 0.01 eV up to nearly 1 eV. For instance, in BCGO, reorientation barriers can take a wide range of different values, starting at less than 0.1 eV for barrier between c-type and d-type sites up to 0.5 eV for barrier between a-type and b-type sites. The same results have been found for In-doped $CaZrO_3$[10] except for the fact that the largest barrier can go up to 0.9 eV.

The very small barrier between c and d sites might explain why position 1c is not considered at all in the work of Bilic and Gale[10] (only seven different positions instead of our eight positions near a specific B atom) and 2c near some specific oxygen atoms O2. According to Table I, 1c and 2c are much higher in energy than nearby positions, that is why the reorientation barriers from c-type site are really small.

In both materials, possible interoctahedral hoppings have a smaller energy barrier than intraoctahedral hopping. This follows from the ability of any oxygen octahedron to bend towards another in the orthorhombic *Pnma* structure, so that two facing oxygens (belonging to different octahedra) can be made very close to each other, but each octahedron remains rigid, so that its own oxygen atoms cannot be made closer to each other (though a little distortion during the transfer is observed, in agreement with previous calculations[3]). Of course, the interoctahedral hoppings are possible only when the oxygen atoms involved are close to each other (this corresponds to a/b type within our notation). The c/d type oxygens, which are made further from each other as a result of the tilting process, are excluded from the interoctahedral motions.

According to those common tendencies, we can suggest that all orthorhombic perovskites behave alike and present as a general but not strict rule the following characteristics: (i) rather low barriers ($\lesssim$0.2 eV) for interoctahedral hopping depending on the level of distortion (barrier is smaller as distortion increases), (ii) higher barriers ($\sim$0.3–0.6 eV) for intraoctahedral hopping, and (iii) a wide range of values for reorientation, from less than 0.1 eV up to 0.8 eV, depending on the type of protonic site.

Finally, there is a quantitative difference between both materials concerning the attractive power of the dopant: it

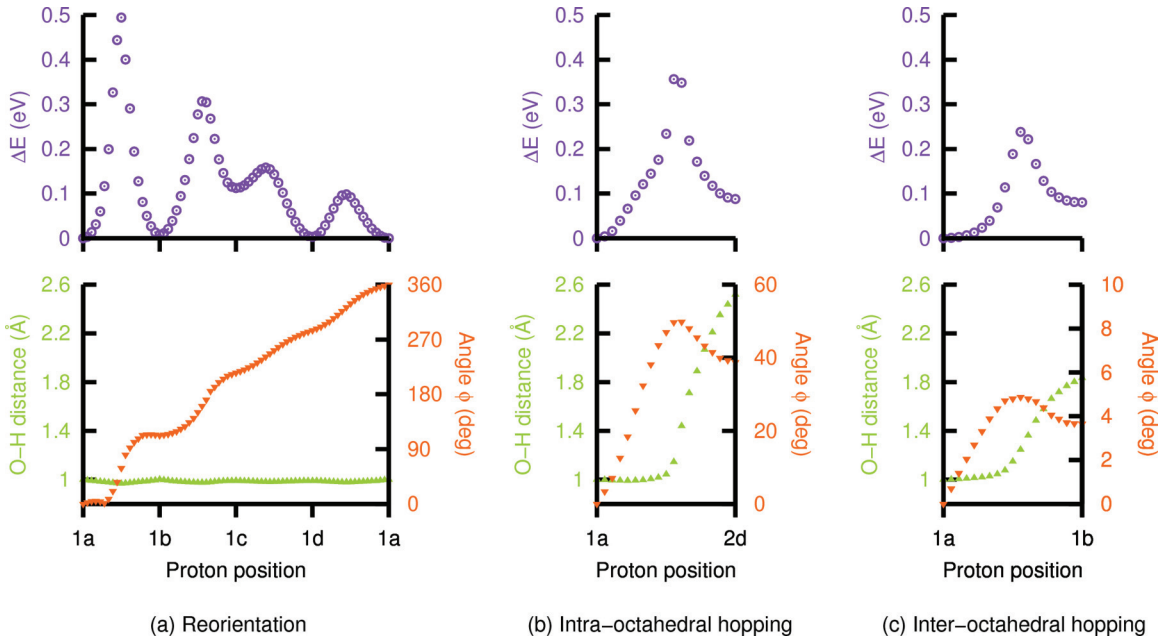

FIG. 4. (Color online) Energy profiles and evolution of some geometric quantities along typical MEP. The angle ϕ is between the initial and current O-H direction.

seems much harder to escape from indium in $CaZrO_3$ than from Gd in $BaCeO_3$. The barrier to escape from indium is on average three times higher than the backward barrier, while in $BaCeO_3$ the escaping barrier is higher only by 50%. This may be due to the nature of the dopant as suggested by Bjorketun *et al.*,[8] which have shown that energy barriers for proton migration near a dopant can be strongly dependent of its nature. Therefore gadolinium seems to be a good candidate as a dopant since its power of attraction is low enough to let the proton escape relatively easily.

B. Rate-limiting events

The energy barriers E_a are not sufficient to discuss the rate-limiting character of the different mechanisms because the associated time scales τ are also dependent on the attempt frequency ν_0 through $\tau \approx \frac{1}{\nu_0} e^{E_a/k_B T}$. ν_0 could be estimated for each energy path by computing the phonon modes in the corresponding stable and saddle point configurations and applying the harmonic transition state theory. Such calculations are, however, computationally very demanding and do not significantly modify the picture provided by the energy barriers alone. Indeed, ν_0 will vary from $\approx$1500 cm^{-1} for the reorientation to $\approx$3000 cm^{-1} for the hopping. Using this difference as a maximum to the uncertainty on the attempt frequency thus leads to an uncertainty of a factor 2 on the time scale, whatever the temperature. By contrast, at $T = 900$ K, the time scale is modified by a factor $\approx$50 when varying the energy barrier from 0.2 eV ($\tau \approx 1.5 \times 10^{-13}$ s) to 0.5 eV ($\tau \approx 7 \times 10^{-12}$ s).

However, the rate-limiting process in such distorted system is not so obvious. Contrary to what can be expected, the reorientation is not necessarily much faster than the hopping. Munch and co-workers have found that the proton transfer step is, indeed, rate-limiting in $BaCeO_3$ but of the same order of magnitude as reorientation for $SrCeO_3$.[39] More precisely, they computed an activation energy for the rotational diffusion in $BaCeO_3$ of 0.07 eV for O_1 and 0.11 eV for O_2, close to the values we get for the lowest reorientation barriers. In earlier work,[45] they found for $Ba\{Ce,Zr,Ti\}O_3$ that reorientation happens much faster with a time scale of $\sim 10^{-12}$ s ($T = 1200$ K), while proton transfer occurs at a time scale of 10^{-9} s ($T = 1200$ K). However, the three materials have been studied in their cubic structure, thus preventing the low-barrier interoctahedral transfer. Gomez and co-workers[42] point out that the rate-limiting process in $SrZrO_3$ (orthorhombic structure) is an intraoctahedral transfer. The fact that most of these studies only focus on the cubic structure might explain why the transfer step has been thought to be rate limiting.

VI. CONCLUSION

In this work, we have performed density-functional calculations on fully hydrated Gd-doped barium cerate and computed in an exhaustive way the MEP between stable protonic sites close and far from the Gd dopant.

Proton transport in perovskites is usually described as a two-step Grotthuss-type diffusion mechanism: a quick reorientation, followed by a transfer to another oxygen.[5] However, even if this is correct in principle, we have found that in Gd-doped $BaCeO_3$, the reorientation is not necessarily a fast process compared to transfer. In this distorted perovskite with orthorhombic *Pnma* space group, interoctahedral hoppings with rather low barriers $\sim$0.2 eV do exist. Also, reorientation mechanisms can be very different from one site to another and thus take a wide range of possible values from 0.02 eV up to 0.54 eV. To a lesser extent, the same argument can be applied to intraoctahedral hopping for which the energy barrier varies between 0.22 and 0.58 eV.

TABLE VI. Comparison of barrier values computed using the doped supercell with the proton "far" from the dopant and a charged undoped $BaCeO_3$.

Barrier	pure $BaCeO_3$		"far" $BaCeGdO_3$	
Reorientation	→	←	→	←
1a-1b	0.54	0.54	0.54	0.54
1b-1c	0.33	0.18	0.33	0.18
1c-1d	0.06	0.15	0.06	0.15
1d-1a	0.09	0.14	0.08	0.14
2a-2b	0.36	0.49	0.36	0.49
2b-2c	0.33	0.17	0.33	0.17
2c-2d	0.03	0.08	0.02	0.08
2d-2a	0.20	0.17	0.20	0.17
Hopping	→	←	→	←
1a-2d	0.50	0.37	0.50	0.37
1b-2d	0.45	0.31	0.45	0.31
1c-2b	0.36	0.47	0.36	0.47
1d-2b	0.42	0.44	0.42	0.44
2a-2c	0.39	0.36	0.39	0.36
1a-1b	0.19	0.20	0.19	0.20
2a-2a	0.21	...	0.21	...
2b-2b	0.16	...	0.16	...

All these results are qualitatively comparable with a previous work focused on the orthorhombic perovskite In-doped $CaZrO_3$.[10] The low barriers found for interoctahedral hopping in these orthorhombic structures suggest that protonic diffusion could be much faster in such structure than in the cubic one, since an interoctahedral hopping is equivalent to two intraoctahedral transfers but with a higher rate. All the barrier values will be exploited in kinetic Monte Carlo simulations to check the actual rate of reorientation versus hopping, and simulate proton trajectories on larger space and time scales.

Finally, gadolinium in barium cerate seems to be interesting as a dopant as it acts like a shallow trap for protons, with rather low escaping barrier (compared to indium in calcium zirconate), enabling the proton to diffuse quite easily. However, other trivalent dopants could be tested to check whether they have better properties for protonic diffusion.

ACKNOWLEDGMENTS

This work was performed using the HPC resources of the TERA-100 supercomputer of CEA/DAM and from GENCI-CCRT/CINES (Grants 2010-096468 and 2011-096468). We acknowledge that some contributions to the present work have been achieved using the PRACE Research Infrastructure resource (machine CURIE) based in France at Bruyères-le-Chatel (Preparatory Access 2010PA0397).

APPENDIX: COMPUTATION OF ENERGY BARRIERS FAR FROM DOPANTS USING A CHARGED SUPERCELL

The barriers corresponding to motions far from the dopant, i.e., from an "f" configuration to another "f" configuration, have been recomputed using an undoped supercell in which the charge of the proton is compensated by a uniform charged background (jellium), as frequently done for the simulation of charged defects. In such cases, there are 16 different motions: eight reorientations, five intraoctahedral hoppings, and three interoctahedral hoppings. This corresponds to 30 barrier values. The energy barriers obtained using this method are compared to the ones obtained using the doped supercell in Table VI: the values obtained using the two methods are the same within 0.01 eV, confirming that a 80-atom supercell is large enough to contain a region "close" to the dopant and a region "far" from it. The proton "far" from the dopant does not feel the influence of Gd atoms, and can be considered as in pure $BaCeO_3$. Besides, the fact that we get the same values in both cases suggests that the jellium only induces a systematic shift in total energies, but does not affect energy differences.

*gregory.geneste@cea.fr

[1] H. Iwahara, T. Esaka, H. Uchida, and N. Maeda, Solid State Ionics **3-4**, 359 (1981).
[2] H. Iwahara, H. Uchida, and S. Tanaka, Solid State Ionics **9-10, Part 2**, 1021 (1983).
[3] M. Cherry, M. Islam, J. Gale, and C. Catlow, J. Phys. Chem. **99**, 14614 (1995).
[4] H. Iwahara, Solid State Ionics **86-88, Part 1**, 9 (1996).
[5] K. D. Kreuer, Solid State Ionics **125**, 285 (1999).
[6] K. D. Kreuer, in *Perovskite Oxide for Solid Oxide Fuel Cells*, edited by T. Ishihara (Springer, US, 2009), pp. 261–272.
[7] T. Norby, in *Perovskite Oxide for Solid Oxide Fuel Cells*, edited by T. Ishihara (Springer, US, 2009), pp. 217–241.
[8] M. E. Björketun, P. G. Sundell, and G. Wahnström, Phys. Rev. B **76**, 054307 (2007).
[9] P. G. Sundell, M. E. Björketun, and G. Wahnström, Phys. Rev. B **76**, 094301 (2007).
[10] A. Bilić and J. D. Gale, Chem. Mater. **19**, 2842 (2007).
[11] J. Hermet, F. Bottin, G. Dezanneau, and G. Geneste, Phys. Rev. B **85**, 205137 (2012).
[12] W. Münch, G. Seifert, K. Kreuer, and J. Maier, Solid State Ionics **86-88**, **Part 1** 647 (1996).
[13] K. D. Kreuer, W. Münch, U. Traub, and J. Maier, Berichte der Bunsengesellschaft für physikalische Chemie **102**, 552 (1998).
[14] W. Münch, K.-D. Kreuer, G. Seifert, and J. Maier, Solid State Ionics **136-137**, 183 (2000).
[15] X. Gonze, B. Amadon, P.-M. Anglade, J.-M. Beuken, F. Bottin, P. Boulanger, F. Bruneval, D. Caliste, R. Caracas, M. Côté *et al.*, Comput. Phys. Commun. **180**, 2582 (2009).
[16] F. Bottin, S. Leroux, A. Knyazev, and G. Zérah, Comput. Mater. Sci. **42**, 329 (2008).
[17] J. P. Perdew, K. Burke, and M. Ernzerhof, Phys. Rev. Lett. **77**, 3865 (1996).
[18] P. E. Blöchl, Phys. Rev. B **50**, 17953 (1994).
[19] M. Torrent, F. Jollet, F. Bottin, G. Zérah, and X. Gonze, Comput. Mater. Sci. **42**, 337 (2008).

[20]W. E, W. Ren, and E. Vanden-Eijnden, Phys. Rev. B **66**, 052301 (2002).
[21]W. E, W. Ren, and E. Vanden-Eijnden, J. Chem. Phys. **126**, 164103 (2007).
[22]Y. Li and G. Wahnström, Phys. Rev. B **46**, 14528 (1992).
[23]Q. Zhang, G. Wahnström, M. E. Björketun, S. Gao, and E. Wang, Phys. Rev. Lett. **101**, 215902 (2008).
[24]V. Barone and C. Adamo, J. Chem. Phys. **105**, 11007 (1996).
[25]P. Goudochnikov and A. J. Bell, J. Phys.: Condens. Matter **19**, 176201 (2007).
[26]K. Knight, Solid State Ionics **145**, 275 (2001).
[27]B.-T. Melekh, V. Egorov, Y. Baikov, N. Kartenko, Y. Filin, M. Kompan, I. Novak, G. Venus, and V. Kulik, Solid State Ionics **97**, 465 (1997).
[28]K.-D. Kreuer, A. Fuchs, and J. Maier, Solid State Ionics **77**, 157 (1995).
[29]R. Hempelmann, M. Soetratmo, O. Hartmann, and R. Wäppling, Solid State Ionics **107**, 269 (1998).
[30]R. Glöckner, M. Islam, and T. Norby, Solid State Ionics **122**, 145 (1999).
[31]R. Davies, M. Islam, and J. Gale, Solid State Ionics **126**, 323 (1999).
[32]T. Tauer, R. O'Hayre, and J. W. Medlin, Solid State Ionics **204-205**, 27 (2011).
[33]E. Matsushita and T. Sasaki, Solid State Ionics **125**, 31 (1999).
[34]M. E. Björketun, P. G. Sundell, G. Wahnström, and D. Engberg, Solid State Ionics **176**, 3035 (2005).
[35]M. A. Gomez, M. A. Griffin, S. Jindal, K. D. Rule, and V. R. Cooper, J. Chem. Phys. **123**, 094703 (2005).
[36]K. Rasim, Ph.D. thesis, Université de Nantes, 2011.
[37]W. Münch, K.-D. Kreuer, G. Seifert, and J. Maier, Solid State Ionics **125**, 39 (1999).
[38]B. Merinov and W. G. III, J. Chem. Phys. **130**, 194707 (2009).
[39]W. Münch, K. D. Kreuer, Adams, G. Seifert, and J. Maier, Phase Transitions **68**, 567 (1999).
[40]M. S. Islam, R. A. Davies, and J. D. Gale, Chem. Mater. **13**, 2049 (2001).
[41]C. Shi, M. Yoshino, and M. Morinaga, Solid State Ionics **176**, 1091 (2005).
[42]M. A. Gomez, S. Jindal, K. M. Fletcher, L. S. Foster, N. D. A. Addo, D. Valentin, C. Ghenoiu, and A. Hamilton, J. Chem. Phys. **126**, 194701 (2007).
[43]Émile Bévillon, A. Chesnaud, Y. Wang, G. Dezanneau, and G. Geneste, J. Phys.: Condens. Matter **20**, 145217 (2008).
[44]A. Bilić and J. D. Gale, Solid State Ionics **179**, 871 (2008).
[45]W. Münch, G. Seifert, K. Kreuer, and J. Maier, Solid State Ionics **97**, 39 (1997).